Interaction of Hydrated Cations with Mica-n (n=2, 3 and 4) Surface.

Esperanza Pavón[1,], Miguel A. Castro[2], Agustín Cota[3], Francisco J. Osuna[2], M. Carolina Pazos[4], María D. Alba[2]*

[1] Unité de Catalyse et de Chimie du Solide, UCCS, CNRS, UMR8181, Université Lille Nord de France, 59655 Villeneuve d'Ascq, France

[2]Instituto Ciencia de Materiales de Sevilla (CSIC-Universidad de Sevilla). Avda. Américo Vespucio, 49. 41092 Sevilla, Spain.

[3]Laboratorio de Rayos-X. CITIUS. Universidad de Sevilla. Avda. Reina Mercedes, 4b. 41012-Sevilla, Spain.

[4] Escuela de Ciencias Químicas, Universidad Pedagógica y Tecnológica de Colombia UPTC. Avda. Central del Norte, Vía Paipa, Tunja, Boyacá, Colombia.

ABSTRACT. High charged swelling micas, with layer charge comprised between 2 and 4, has been found to readily swell with water and that complete cation exchange (CEC) can be achieved. Due to their high CEC, applications like radioactive cation fixation or removal of heavy metal cations from waste water were proposed. Their applicability can be controlled by the location of the interlayer cation in a confined space with a high electric field. In synthetic brittle micas, the interlayer cation has a low water coordination number; therefore their coordination sphere would be completed by the basal oxygen of the tetrahedral layer as inner-sphere complexes (ISC). However, no direct evidence of these complexes formation in brittle micas has been reported yet. In this contribution, we mainly focus on the understanding the mechanisms that provoke the formation of ISC in high charge swelling micas, Mica-n. A whole series of cations (X) were used to explore the influence of the charge and size of the interlayer cation. Three brittle swelling micas, Mica-n (n=4, 3 and 2), were selected in order to analyze the influence of the layer charge in the formation of ISC. The contribution of the ISC has been analyzed thorough the evolution of the 060 reflection and the changes in the short-range order of the tetrahedral cations will be followed ^{29}Si and ^{27}Al MAS-NMR. The results showed that ISC was favored in X-Mica-4 and that provoked a high distortion angle between the Si-Al tetrahedra. When the content of aluminum decreases, the electrostatic forces between the layers are relaxed, and the hydrated cations did not interact so strongly with the tetrahedral sheet, having the opportunity to complete their hydration sphere.

2

TOC GRAPHIC
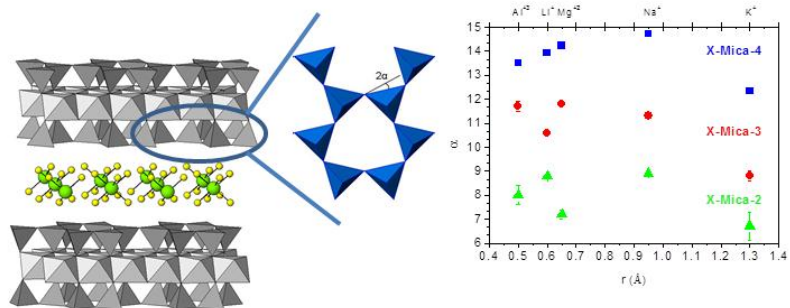
INTRODUCTION

High charge swelling micas, with layer charge comprised between 2 and 4, has been found to readily swell with water and that complete cation exchange (CEC) can be achieved.[1,2,3,4,5,6,7] Due to their high CEC (theoretically up to 468 meq/100g), applications like radioactive cation fixation or removal of heavy metal cations from waste water were proposed.[8,9,10,11,12,13]

In those high charged synthetic micas, the layers bear a high permanent negative charge compensated by counterions located between them (interlayer space). These counterions are the origin of two interesting features: mica swelling and cationic exchange. The former refers to the uptake of water into the interlayer space, while the latter involves the replacement of original counterions Na^+ by cations of aqueous solution.[14,15,16,17] Both processes will be controlled by the location of the interlayer cation in a confined space with a high electric field.

Recently, two important items related to these swelling brittle micas have been reported 1) the interlayer cations do not exchange completely.[18] 2) The water coordination of the cations is small to full fill their hydration sphere.[19]

The hydration state of the interlayer cations has been shown to depend on both the layer charge of the aluminosilicate and the nature of the interlayer cation.[19] In synthetic brittle micas, the interlayer cation has a low water coordination number; therefore their coordination sphere would be completed by the basal oxygen of the tetrahedral layer as inner-sphere complexes (ISC). This fact has been found as well in the hectorite surface, where weakly solvated ions, such as K^+, are able to form ISC.[20] However, no direct evidence of these complexes formation in brittle micas has been reported yet.

In this contribution, we mainly focus on the understanding the mechanisms that provoke the formation of ISC in high charge swelling micas, Mica-n. In terms of methodology, we draw attention to the relation between the hexagonal hole in the tetrahedral layer and the interlayer cation, which allows detailed understanding of both the confined cation and the clay surface structure. Then, a whole series of cations will be used to explore the influence of the charge and

size of the interlayer cation. Three brittle swelling micas, with different Si/Al ratio, were selected in order to analyze the influence of the layer charge in the formation of ISC. The contribution of the ISC will be analyzed thorough the evolution of the 060 reflection and the changes in the short-range order of the tetrahedral cations will be followed ^{29}Si and ^{27}Al MAS-NMR

EXPERIMENTAL

Synthesis Method

A procedure similar to that described by Alba et al.[21] was employed. Near-stoichiometric powder mixtures with the molar compositions (8 - n) SiO_2, (n/2) Al_2O_3, 6 MgF_2, and (2n) NaCl were used to synthesize Na-Mica-n (n = 2, 3, 4). The starting materials were SiO_2 from Sigma (CAS no. 112945-52-5, 99.8% purity), $Al(OH)_3$ from Riedel-de Haën (CAS no. 21645-51-2, 99% purity), MgF_2 from Aldrich (CAS no. 20831-0, 98% purity), and NaCl from Panreac (CAS no. 131659, 99.5% purity). All reagents were mixed and vigorously grounded before heating up to 900 °C in a Pt crucible for 15 h. After cooling, the solids were washed with deionized water and dried at room temperature. The as-synthesized samples are named Na-Mica-n (n ranging between 2 and 4). XRF analyses were carried out in order to check the chemical composition of these samples (see "Sample Characterization" session for acquisition details). The results are displayed in Table 1, as well as the Si/Al ratio achieved compared with the theoretical value. A good accurate is obtained and allows us affirming that chemical compositions of these samples are close to the theoretical one. The as-made solids were analyzed by X-ray Diffraction (XRD) to evaluate their purity (Figure 1S, Supporting Information).

Cation-Exchange Process

The as-synthesized Na-Mica-n were exchanged with solutions of Li^+, K^+, Mg^{+2} and Al^{+3} salts at concentrations that ensured that the molar amount of cation was 10 times the cation-exchange capacity (CEC) of the mica.[19] The most important characteristics of these

5

ions in solution are displayed in Table 2. The reagents used were $MgCl_2$ from Sigma-Aldrich (CAS n° 7786-30-6, 99.99% purity), KCl from Fluka (CAS n° 7447-40-7, >99% purity), $AlCl_3$ from Fluka (CAS n° 7784-13-6, >99.0 % purity), and LiCl from Fluka (CAS n° 7447-41-8, >99.0% purity). Ion-exchange process was described elsewhere.[19] The resulting solids were analyzed by X-ray Diffraction (XRD) to evaluate the purity of the samples (Figure 2S, Supporting Information). This exchange method prevents the modification of the silicate framework and consequently, XRF analyses were not needed. The extent of the cation exchange reaction was monitored by ^{23}Na MAS- NMR. These solids are referred to as X-Mica-n, where $X=Na^+$, Li^+, K^+, Mg^{+2}, or Al^{+3} and n=2, 3, or 4.

Sample Characterization.

X-ray diffraction (XRD) patterns were measured at the CITIUS X-ray laboratory (University of Seville, Spain) using a Bruker D8 Advance instrument equipped with a Cu K_α radiation source, operating at 40 kV and 40 mA, and with a Ni filter. The powder XRD patterns were registered in the 2θ-range 58–62° with a step size of 0.05° and a time step of 20 s. The analysis of the peaks were carried out using TOPAS© from Bruker© and Pseudovoight functions.

XRF of powdered samples in borate flux was performed to obtain information about the chemical composition of the samples. XRF measurements were made with an automated Philips PW1400 spectrometer at the CITIUS, Universidad de Sevilla.

^{29}Si and ^{27}Al (SP) MAS-NMR spectra were recorded at the Spectroscopy Service of ICMS (CSIC-US, Seville, Spain) using a Bruker DRX400 spectrometer equipped with a multinuclear probe. Powdered samples were packed in 4-mm zirconia rotors and spun at 10 kHz. ^{29}Si MAS-NMR spectra were acquired at 79.49 MHz, using a pulse-width of 2.7 μs (π/2=7.1 μs) and a pulse space of 3 s. ^{27}Al (SP) MAS-NMR spectra were recorded at 104.26

MHz, using a pulse width of 0.92 μs (π/2=9.25 μs) and a pulse space of 0.1s. The chemical shift values are reported in ppm with respect to tetramethylsilane for ^{29}Si and AlCl₃ 0.1M for ^{27}Al.

RESULTS AND DISCUSSION

Hexagonal cavity distortion: b parameter

In all the samples, the 060 reflections (Figure 1) are in the 2θ range between 59.5 to 60.2º which is typical of trioctahedral clays[22] and the 2θ value depend on the interlayer cation (Table 2).

The distance associated to this reflection, $d_{(060)}$, (Table 2) depends on the composition of the octahedral sheet, the amount of Al in tetrahedral sheet and the degree of tetrahedral tilt angle.[22] For these reasons, trioctahedral clays like saponite and vermiculite exhibit a higher value (1.52 and 1.54 Å, respectively) than dioctahedral clay such as montmorillonite ($d_{(060)}$ =1.49-1.50 Å). The values obtained for our samples ranges between 1.50 to 1.56 Å. The biggest values, found for the highest charge micas (n=4 and 3), are closer to the values reported for vermiculites, whereas for n=2, $d_{(060)}$ is in the reported value for trioctahedral micas, like Biotite (1.538 Å).

Geometry considerations can be derived from the 060 reflection (Table 2). For most of the layered silicate, the ideal hexagonal cavity (Figure 2a) is distorted to a ditrigonal symmetry by the oppose rotation of alternate tetrahedron (Figure 2.b). The amount of this rotation varies from a few degrees to near the theoretical maximum of 30º. This tetrahedral rotation has been attributed to the difference in size between the tetrahedral and octahedral sheets (the first one is higher than the second).[23,24] The average tetrahedral rotation from

hexagonal symmetry, α, may be predicted from the observed *b* axis and the known Al-for-Si substitution as:[22]

$$\cos \alpha = \frac{b_{obs}}{b_{theor}} \qquad (1)$$

where b_{theor} is the value obtained from[25] $b_{(Si_{4-x}Al_4)} = 9.15 + 0.74x, \dot{A}$, (*x* is the theoretical grade of substitution of Si^{4+} for Al^{3+} in the tetrahedral sheet) and b_{obs} is the experimental value calculated form $d_{(060)}$ distance, taking into account that in monoclinic cells, b=6· $d_{(060)}$, Å.

From the experimental $d_{(060)}$ values and the sample chemical compositions, the distortion angle, α and *b parameter* were calculated (Table 2) and have been correlated to the interlayer cation size (Figure 3).

The maximum distortion is found for the samples with the highest isomorphical substitution Si/Al and hence, highest layer charge (upper blank triangle, Figure 3). This behavior is a consequence of the inhibition of the incorporation of the water molecules to the interlayer space when layer charge increase.[19] In such case, the interlayer cations are less hydrated and increase the contribution of inner sphere complex. As observed in the Figure, the distortion created increases with the increase in the ionic radii of the interlayer cation, meaning that in this case, where ISC are favored to occur, the radii of the interlayer cation is the parameter that influence in the grade of distortion produce in the layer. The sample homoinized by K^+ is the only exception in this behavior. This case will be analyzed further in the following section (see ^{29}Si NMR).

On the opposite site, when layer charge decreases, the electrostatic interaction between the layers is relaxed and allows the hydration of the interlayer cations.[19] This fact hinders the contribution of inner sphere complexes and consequently, smaller distortion in the tetrahedral

sheet are expected as occurred for samples n=3 and n=2. In this case, the influence of the ionic radii in the distortion is smaller.

In X-Mica-n, the interlayer cations are housed in the hexagonal cavities formed by the O^{2-} anions of the opposite tetrahedral sheets (Figure 2c). Therefore, disregarding distortions, these cations have 12-fold coordination, and the bond length between oxygens and interlayer cations, *d*, can be calculated through the equation:

$$d = \sqrt{\frac{h^2}{4} + r^2} \qquad (2)$$

where *h* is the interlayer space, $h=d_{001}-9.4$, Å and *r* is de distance from the centre of the hexagonal cavity to the oxygens of the plane in a tetrahedral sheet. In case of the tetrahedral sheets deformation by rotation of angle α, *r* varies as follows:[26]

$$r = \frac{b}{6\cos 30} - \frac{b\tan\alpha}{6} = \frac{b}{6}\left(\sqrt{3} - \tan\alpha\right) \qquad (3)$$

Bond distance between the basal oxygens and the interlayer cations calculated using eq. 2 are also displayed in Table 2. To determine these parameters the interlayer space is required (calculated using the d_{001} distance, Table 2).[19]

The distance between the basal oxygens and the centre of the hexagonal cavity, *r*, slightly differs from the expected range (2.6 Å)[27]. Shortest distances are obtained when n=4, and the presence of ISC is encouraged. However, when layer charge decreases, this distance increases reflecting the smaller distortion provoked by the interlayer cations, although it never arrives to the ideal value.

The distance between the interlayer cation and the basal oxygens (*d*) when a monolayer of water is considered[24] ($d_{001}≈12$ Å) range between 2.6 and 3.4 Å. In the case n=4, the distance is smaller (between 2.6 and 3.08 Å) indicating that hexagonal cavities are

9

deformed to accommodate the cation but holding an optimal equilibrium distance between the interlayer cation and the basal oxygens. When layer charge decrease, and hence, the interlayer cations are able to hydrated easily, the contribution of inner sphere complex is smaller and hence, a longer distance between the interlayer cations and the basal oxygens is observed (Table 2).

Influence of the ISC in the ^{29}Si/^{27}Al tetrahedral framework. ^{29}Si MAS NMR Spectroscopy

Figures 4 and 5 show the ^{29}Si (SP) MAS NMR spectra for the X-Mica-n homoionized with the alkaline cations (Figure 4) and with the cations from the third period of the periodic table (Figure 5). In general, these spectra can be described as a wide band in the range between -70 ppm and -95 ppm, associated to Q^3 (mAl) with $0 \leq m \leq 3$ environments on phyllosilicates 2:1 (marked with asterisks in the Figures 4 and 5)[2,21,32,28,29,30,31]. The differences observed in the registered spectra can be summarized as follow:

- When layer charge decreases, a shift is observed in all the Q^3(mAl) signals to lower frequencies, accompanied by a different relative intensities of the signals, consequence of the different quantity of Q^3(mAl) expected in the micas.

- A new contribution at -85 ppm (discontinuous line in X-Mica-2 and X-Mica-3) is observed in all the samples. It corresponds to sodalite, a reaction product already observed by XRD diffraction[32] and more evident in the lower layer charge samples.

- A fifth peak at -75 ppm is observed in the samples with a layer charge n=4 (dashed line in X-Mica-4). The assignment of this peak is still not solved: if Lowenstein's rule is considered, only one ^{29}Si peak will be present in the

spectra, as the Si/Al ratio in these samples is 1. However, more than one peak is observed in the spectra, so a non-homogeneous distribution is involved, and then, the existence of Al-O-Al bonds can be possible, Lowenstein's rule being violated. The presence of this peak in all the silicates makes this theory stronger. However, it also can be assigned to other non-crystalline phases that cannot be observed by XRD. For the silicates with lower layer charge, this contribution is not observed, motivated by the smaller isomorphous substitution of Si^{4+} by Al^{+3}.

- In the X-Mica-4, ^{29}Si peaks shift to higher frequencies values when the ionic radius of the cations increases. In the samples with lower layer charge, this displacement is also shown, but it is smaller than in the highest charged mica, due to the lower cations concentration in the interlayer space and their highest distance with the basal plane.

The local order of the silicon atoms in swelling silicates as smectites and vermiculites, were not affected by the presence of the hydrated interlayer cation[31]. The local environment of silicon was found to be affected after the dehydration of the interlayer cations. In fact, dioctahedral mica with Al^{+3} isomorphous substitution in the tetrahedral sheet and similar layer charge show variations in the ^{29}Si chemical shifts values for $Q^3(0Al)$ up to 1.6 ppm[31]. This behavior was attributed to the tetrahedral rotation, α, due to the different ionic radii of the interlayer cations. Because Na^+ (1.02 Å in 6-fold coordination[33]) is smaller than K^+ (1.37 Å in 6-folf coordination[33]), the oxygen framework rotates slightly to coordinate more closely with Na^+, which causes a larger α value and producing a slightly less shielded ^{29}Si chemical shift. These distortions also allowed the interlayer cation to be 6-fold coordinated by oxygens. However, the effect of exchangeable hydrated cations appears to be small even when Cs^+ was the interlayer cation[33]. Similar results have been found by Thompson[34] in montmorillonites.

Taking into account that in X-Mica-n the interlayer cations are hydrated, the shifts of the ^{29}Si MAS-NMR signals can only be explained by the formation of Inner Sphere Complexes between the formers and the tetrahedral layer of the silicate to complete their coordination sphere which was observed by TG analysis being incomplete.[19] To analyze the ability that the hydrated interlayer cations have to form an inner sphere complex, the chemical shifts of the four environments of the ^{29}Si have been analyzed as a function of their ionic radii (Figure 6).

All the ^{29}Si signals shift toward higher frequencies when the ionic radii increase as the distortion angle α also do (Table 2). Samples exchanged with K^+ constituted the only exception: chemical shifts are displaced to lower frequency values respect Na^+ and Li^+, meaning that the shielding produce for this cation in the environment of Si is smaller.

Based on the Pearson´s theory[35,36,37] for the formation of solution-phase complexes, the cation-exchange selectivity is defined in terms of attractive forces between the cations and the clay surface, being the operating forces the polarizability-based electrostatic, van der Waals, and even covalent interactions. Consequently, the siloxane ditrigonal cavitites on the basal surfaces of clays minerals act as polarizable Lewis bases, and thus preferentially form inner-sphere complexes with more polarizable (softer) Lewis acids.[38],[39]

Therefore, the tendency of forming ISC in these clay materials would depend on the acidity of the interlayer cation, and hence should follow the trend $K^+ > Na^+ > Mg^{+2} > Li^+ > Al^{+3}$, or $K^+ > Na^+ > Li^+$ considering the cation from the first group, and $Na^+ > Mg^{+2} > Al^{+3}$ considering the third period cations. The position of the signals in the ^{29}Si NMR spectra reveals that the shielding produced for these cations in the silicon surrounding follow this rule as well.

However, the results obtained with the K^+ ions, specially for the Q^3 (3Al) environment show that, even if it is the softer Lewis acid used, the samples homoionized with this cation does not exhibit the highest tendency of forming inner-sphere complexes, as

revealed by the smallest shielding in ^{29}Si NMR results. Steric effects contribute to explain this behavior. A larger hydrated radius means that the cationic center of charge is farther from the clay surface so the clay-cation electrostatic interaction is weaker.[38]

In addition, silicate layer charge also affects the formation of the ISC. When layer charge increases, the negative charge in the surface also increases, and therefore, the materials turn out to be more polarizable Lewis bases. As a result, a bigger tendency on forming ISC is found and the effect of the interlayer cation is less evident, as can be seen in the displacement range of the ^{29}Si chemical shift positions (Figure 6).

^{27}Al MAS NMR Spectroscopy

To improve the knowledge of the tetrahedral sheet of X-n-Mica, ^{27}Al MAS-NMR spectra were registered (Figure 7). All the spectra show an asymmetric band at ca. 67 ppm corresponding to aluminum in tetrahedral coordination[30]. Likewise, a peak centered at ca. 0 ppm, arising from octahedral coordination, is only observed in the high charge micas[30] or the micas homoionized with aluminum.

Regarding tetrahedral environments, ^{27}Al MAS-NMR spectra show two components which have been previously identified, although they have not been interpreted due to the quadrupolar nature of Al[21,40]. However, changes in the FWHM values of the spectra are observable. X-Mica-4 exhibit broader spectra than the lower charged silicates. This can be explained by the distortion exerted on the tetrahedral aluminum as consequence of the location of the interlayer cation in the pseudohexagonal cavity. Although this fact has never been seen in hydrated clays, it has been already reported for Li-montmorillonite heated at 300ºC.[41,42]

On the other hand, Al in octahedral coordination could be due to a partial substitution of Mg^{+2} by Al^{+3} in the octahedral sheet or as interlayer cation. The signals coming in the high

charge silicates in the octahedral region are very similar in all the spectra, suggesting that the Al^{+3} are in the octahedral sheet, not in the interlayer space, also according with the literature[40]. Samples homoionized with Al^{+3}, however, show a clear narrow peak in the octahedral region, meaning that in those cases, aluminum is hexacoordinated in the interlayer space of the silicates. There is no clear relationship between the aluminum in this environment and the interlayer cation, as a consequence of the length distance between them.

CONCLUSIONS

For the first time, the formation ISC in the interlayer space of the family of swelling high charged mica has been demonstrated. Moreover, the results have helped to clarify the interactions and disruption that the interlayer cations provoke in the tetrahedral sheet of a series of high charge swelling silicates. When the ratio Si/Al was one, Inner Sphere Complexes are favored and that provokes a high distortion angle between the Si-Al tetrahedra. When the content of aluminum decreases, the electrostatic forces between the layers are relaxed, and the hydrated cations do not interact so strongly with the tetrahedral sheet, having the opportunity to complete their hydration sphere.

AUTHOR INFORMATION

Corresponding Author

*Phone: +33 0320335907. E-mail: epavon@us.es

Notes

The authors declare no competing financial interest

Supporting Information: This information is available free of charge via the Internet at http://pubs.acs.org

REFERENCES

(1) Alba, M.D.; Castro, M.A.; Naranjo, M.; Orta, M.M.; Pavon, E.; Pazos, M.C. Evolution of Phases and Al-Si Distribution during Na-4-Mica Synthesis. *J Phys. Chem. C.* **2011**, *115*, 20084-20090.

(2) Park, M.; Lee, D.H.; Choi, C.L.; Kim, S.S.; Kim, K.S.; Choi, J. Pure Na-4-mica: Synthesis and Characterization. *Chem. Mater.* **2002**, *14*, 2582-2589.

(3) Alba, M.D.; Castro, M.A.; Naranjo, M.; Pavón, E. Hydrothermal reactivity of Na-n-Micas. *Chem. Mater*. **2006**, *18*, 2867-2872.

(4) Taruta, S.; Kaga, T.; Yamaguchi, T.; Kitajima, K. Thermal transformation and ionic conductivity of ammonium ion-exchanger prepared from Na-4-mica. *Mater. Sci. Eng B* **2010**, *173*, 271-274.

(5) Komarneni, S.; Ravella, R.; Park, M. Swelling mica-type clays: synthesis by NaCl melt method, NMR characterization and cation exchange selectivity. *J. Mater. Chem.* **2005**, *15*, 4241-4245.

(6) Bedelean, H.; Maicaneanu, A.; Burca, S.; Stanca, M. Removal of heavy metal ions from wastewaters using natural clays. *Clay Miner.* **2009**, *44*, 487-495.

(7) Kodama, T.; Harada, Y.; Ueda, M.; Shimizu, K.; Shuto, K.; Komarneni, S.; Hoffbauer, W.; Schneider, H. Crystal-size control and characterization of Na-4-mica prepared from kaolinite. *J. Mater. Chem*. **2001**, *11*, 1222-1227.

(8) Kodama, T.; Komarneni, S. Na-4-mica: Cd^{2+}, Ni^{2+}, Co^{2+}, Mn^{2+} and Zn^{2+} ion exchange. *J. Mater Chem.* **1999**, *9*, 533-539.

(9) Paulus, W.J.; Komarneni, S.; Roy, R. Bulk synthesis and selective exchange of strontium ions in $Na_4Mg_6Al_4Si_4O_{20}F_4$ Mica. *Nature*. **1992**, *357*, 571-573.

(10) Kodama, T.; Komarneni, S. Alkali metal and alkaline earth metal ion exchange with Na-4-mica prepared by a new synthetic route from kaolinite. *J. Mater Chem.* **1999**, *9*, 2475-2479.

(11) Brigatti, M.F.; Colonna, S.; Malferrari, D.; Medici, L.; Poppi, L. Mercury adsorption by montmorillonite and vermiculite: a combined XRD, TG-MS, and EXAFS study. *Appl. Clay Sci.* **2005**, *28*, 1-8.

(12) Kodama, T.; Komarneni, S.; Hoffbuauer, W.; Schneider, H. Na-4-mica: simplified synthesis from kaolinite, characterization and Zn, Cd, Pb, Cu and Ba uptake kinetics. *J. Mater. Chem.*, **2000**, *10*, 1649-1653.

(13) Noh, Y.D.; Komarneni, S. Mercury(II) Exchange by Highly Charged Swelling Micas, Sodium Engelhard Titanosilicate-4, and Sodium Titanosilicate. *Environ. Sci. Technol.*, **2011**, *45*, 6954-6960.

(14) Slabaugh, W.H. Cation exchange properties of bentonite. *J. Phy. Chem.* **1954**, *58*, 162-165

(15) Barrer, R.M.; Brumer, K. Relations between partial ion exchange and interlamellar sorption in alkylammonium montmorillonites. *Trans. Faraday Soc.* **1963**, *59*, 959-968

(16) Mae, A., Cremers, A. Site group-interaction effects in zeolite-y .2. Na-Ag selectivity in different site groups. *Faraday Trans. 1.* **1978**, *74*, 1234-1241

(17) Dyer, A.; Chow, J.K.K.; Umar, I.M. The uptake of caesium and strontium radioisotopes onto clays. *J. Mater. Chem.* **2000**, *10*, 2734-2740.

(18) Tenório, R.P.; Alme, L.R.; Engelsberg, M.; Fossum, J.O.; Hallwass, F. Geometry and Dynamics of intercalated water in na-Fluorhectorite Clay Hydrates. *J. Phys. Chem. C.* **2007**, *112*, 575-580.

(19) Pavón, E.; Castro, M.A.; Naranjo, M.; Orta, M.M.; Pazos, C.; Alba, M.D. Hydration properties of synthetic high-charge micas saturated with different cations: An experimental approach. *Am. Miner.* **2013**, *98*, 394-400.

(20) Skipper, N.T.; Lock, P.A.; Titloye, J.O.; Swensom, J.; Mirza, Z.A.; Howells, W.S.; Fernandez-Alonso, F. The structure and dynamics of 2-dimensional fluids in swelling clays. *Chem. Geol.* **2006**, *230*, 182–196.

(21) Alba, M.D.; Castro, M.A.; Naranjo, M.; Pavón, E. Hydrothermal reactivity of Na-n-Micas. *Chem. Mater.* **2006**, *18*, 2867-2872.

(22) Moore, D.M.; Reynolds R.C. *X-Ray Diffraction and the Identification and Analysis of Clay Minerals.* Ed Oxford University Press, **1997**.

(23) Brindley, G.W.; Brown, G. *Crystal Structures of Clay Minerals and their X-Ray Identification.* Mineralogical Society, London, UK, **1980**.

(24) Newman, A.C.D. *Chemistry of Clays and Clay Minerals*, Wiley, New York, USA, **1987**.

(25) Méring, J. *Smectites*. In. Gieseking J.E (ed) Soil components, vol 2 : Inorganic components. Springer, Berlin Heidelberg, New York, **1975**, pp 97-119

(26) Decarreau, A. *Materiaux argileux. Structure, propiétés et applications.* Soc. Fr. Mineral Cristall, Paris, **1990**, pp 586

(27) Sposito, G.; Skipper, N.; Sutton, R.; Park, S.H.; Soper, A.; Greathouse, F. Surface geochemistry of the clay minerals. *Proc. National Academy of Sciences of the United States of America*, **1999**, *96*, 3358-3364.

(28) Engelhardt, M.D. *High Resolution Solid State NMR of Silicates and Zeolites.* John Wiley and Sons, New York, **1987.**

(29) Mackenzie, K.J.D.; Smith, M.E. *Multinuclear Solid State NMR of Inorganic Materials*. Elservier Science Ltd, Oxford, **2002**.

(30) Sanz, J.; Sarratosa, J.M. Si-29 and Al-27 high resolution MAS-NMR spectra of phyllosilicates. *J. Amer. Chem. Soc.* **1984**, *106*, 4790-4793.

(31) Weiss, C.A.; Altaner, S.P.; Kirkpatrick, R.J. High-resolution ^{29}Si NMR spectroscopy of 2:1 layer silicates: correlations among chemical shifts, structural distortions and chemical variations. *Am. Miner.* **1987**, *72*, 935-942.

(32) Alba, M.D.; Castro, M.A.; Naranjo, M.; Orta, M.M.; Pavón, E.; Pazos M.C. Evolution of phases and Al-Si distribution during Na-4-mica synthesis. *J. Phys. Chem. C* **2011**, *115*, 20084-20090.

(33) Shannon, R.D.; Prewitt, C.T. Effective ionic radii in oxides and flourides. *Acta Crystal. B.* **1969**, *25*, 925-946.

(34) Thompson, J.G. ^{29}Si and ^{27}Al nuclear magnetic resonance spectroscopy of 2:1 clay minerals. *Clay Miner.* **1984**, *19*, 229-236.

(35) Pearson, R.G. Hard and soft acids and bases. *J. Am. Chem. Soc.* **1963**, *85*, 3533-3539.

(36) Pearson, R.G. Hard and soft acids and bases, HSAB, part I: Fundamental principles. *J. Chem. Educ.* **1968**, 581-586.

(37) Pearson, R.G. Hard and soft acids and bases, HSAB, part II: Underlying theories. *J. Chem. Educ.* **1968**, 643-648.

(38) Shainber, I.; Kemper, W.D. Ion exchange equilibria on montmorillonite. *Soil Sci.* **1967**, *103*, 4-9.

(39) Bolt, G.H.; Kemper, W.D.; Shainber, I. Discussion of paper by Shainberg, I and Kemper, WD entitled ion exchange equilibria on montmorillonite. *Soil Sci.* **1967**, *104*, 444-453.

(40) Komarneni, S.; Pidugu, R.; Amonett, J.E. Synthesis of Na-4-Mica from metakaolinite and MgO: characterization and Sr^{+2} uptake kinetics. *J. Mater. Chem.* **1988**, *8*, 205-208.

(41) Trillo, J.M.; Alba, M.D.; Alvero, R.; Castro, M.A. Rexpansion of collapsed Li-Montomorillonites. Evidence of the location of Li$^+$ ions. *J. Chem. Soc. Chem. Comm.* **1993**, *24*, 1809-1811.

(42) Trillo, J.M.; Alba, M.D.; Alvero, R.; Castro, M.A. Reversible migration of lithium in montmorillonites. *J. Phys. Chem.* **1994**, *98*, 7484-7853.

Table 1. Elemental quantification obtained by XRF analysis for the three initial samples.

	%						
	Na (±0.09)	Al (±0.4)	Mg (±0.06)	Si (±0.09)	F (±0.3)	Si/Al	Si/Al theor
Na-Mica-4	7.95	6.1	17.10	18.95	13.5	1.04	1
Na-Mica-3	9.46	9.0	16.75	15.67	14.3	1.74	1.68
Na-Mica-2	9.46	12.4	17.30	12.91	11	3.1	3

Table 2. Physicochemical properties of cations. *r* represents the Pauling ionic radius, *q/r* is the relation between the ionic charge and ionic radius. *ΔH⁰hyd* is the hydration enthalpy and *pKₐ* is the acidity constant.

	K^+	Na^+	Li^+	Mg^{+2}	Al^{+3}
r (Å)	1.33	0.95	0.6	0.65	0.5
q/r	0.75	1.05	1.70	3.08	6.00
ΔH^0_{hyd}(KJ/mol)	-305	-406	-519	-1922	-4660
pK_a	14.5	14.2	13.6	11.4	5.0

Table 3. 060 and 001 planar distance, b-parameter, distortion tetraedra angle (α) and cation-basal plane distance of X-Mica-n.

Cation (X)	060/2θ	d_{060} (Å)	d_{001}(Å)	b_{obs}(Å)	α	r(Å)	d(Å)
			X-Mica-4				
Li^{+}	59.75±0.01	1.55±0.01	11.96±0.02	9.28±0.05	13.92±0.02	2.30±0.05	2.63±0.05
Na^{+}	59.99±0.01	1.54±0.01	12.17±0.01	9.25±0.04	14.71±0.02	2.26±0.03	2.65±0.03
K^{+}	59.33±0.02	1.56±0.03	12.83±0.02	9.30±0.20	12.33±0.08	2.40±0.20	2.90±0.10
Mg^{+2}	59.84±0.02	1.54±0.03	12.06±0.02	9.30±0.20	14.23±0.09	2.30±0.20	2.60±0.20
Al^{+3}	59.69±0.01	1.55±0.02	13.50±0.02	9.30±0.10	13.50±0.02	2.30±0.10	3.08±0.08
			X-Mica-3				
Li^{+}	59.80±0.01	1.55±0.02	12.13±0.02	9.27±0.09	10.60±0.04	2.29±0.09	2.80±0.30
Na^{+}	59.97±0.01	1.54±0.02	12.17±0.01	9.30±0.10	11.31±0.04	2.36±0.09	2.74±0.08
K^{+}	59.45±0.06	1.55±0.08	12.80±0.04	9.32±0.50	8.80±0.20	2.50±0.50	3.00±0.40
Mg^{+2}	60.06±0.03	1.54±0.05	14.27±0.02	9.20±0.30	11.80±0.10	2.40±0.30	3.40±0.20
Al^{+3}	60.06±0.05	1.54±0.07	14.05±0.04	9.20±0.40	11.70±0.20	2.40±0.40	3.30±0.30
			X-Mica-2				
Li^{+}	60.34±0.02	1.53±0.03	12.11±0.03	9.20±0.20	8.80±0.10	2.40±0.30	3.40±0.20
Na^{+}	60.36±0.01	1.53±0.02	12.17±0.01	9.20±0.20	8.90±0.07	2.40±0.10	2.80±0.10
K^{+}	60.02±0.07	1.50±0.10	12.86±0.02	9.20±0.60	6.70±0.60	2.00±0.10	3.10±0.10
Mg^{+2}	60.13±0.02	1.54±0.03	14.34±0.03	9.20±0.30	7.20±0.20	2.50±0.30	3.50±0.20
Al^{+3}	60.21±0.06	1.50±0.10	13.94±0.02	9.20±0.30	8.00±0.40	2.40±0.70	3.30±0.50

FIGURE CAPTIONS

Figure 1. X-ray diffraction diagrams in the range of the 060 reflection. Asterisks represent the peak used in the following calculations (Table 2).

Figure 2. a) Projection of the *ab* plane of the tetrahedral sheet. Continuous line represents the Bravais unit cell and the discontinuous line represents the primitive cell. b) Tetrahedral sheet distortion due to the α-rotation of adjacent tetrahedra. c) Distance between the apical oxygens and the interlayer cations.

Figure 3. Distortion angles calculated from the b parameter obtained from the 060 reflection versus the interlayer cation radius. Squares= X-Mica-4, circles = X-Mica-3 and triangles= X-Mica-2.

Figure 4. ^{29}Si MAS-NMR spectra of X-Mica-n as a function of the layer charge (n) for the alkaline interlayer cations: a) Li^+, b) Na^+, and, c) K^+. Q^3(mAl) environments are marked with *

Figure 5. ^{29}Si MAS-NMR spectra of X-Mica-n as a function of the layer charge (n) for the third period interlayer cations: a) Na^+, b) Mg^{2+}, and, c) Al^{3+}. Q^3(mAl) environments are marked with *

Figure 6. ^{29}Si chemical shift values obtained from the fit of the spectra of the Figures 4 and 5 in function of the interlayer cation radius. Q^3(mAl) m=3, 2, 1 and 0 are represented by squares, circles, upper triangle and downer triangle respectively, and are separated by dot lines. Solid symbols=X-Mica-4, crossed=X-Mica-3 and open=X-Mica-2.

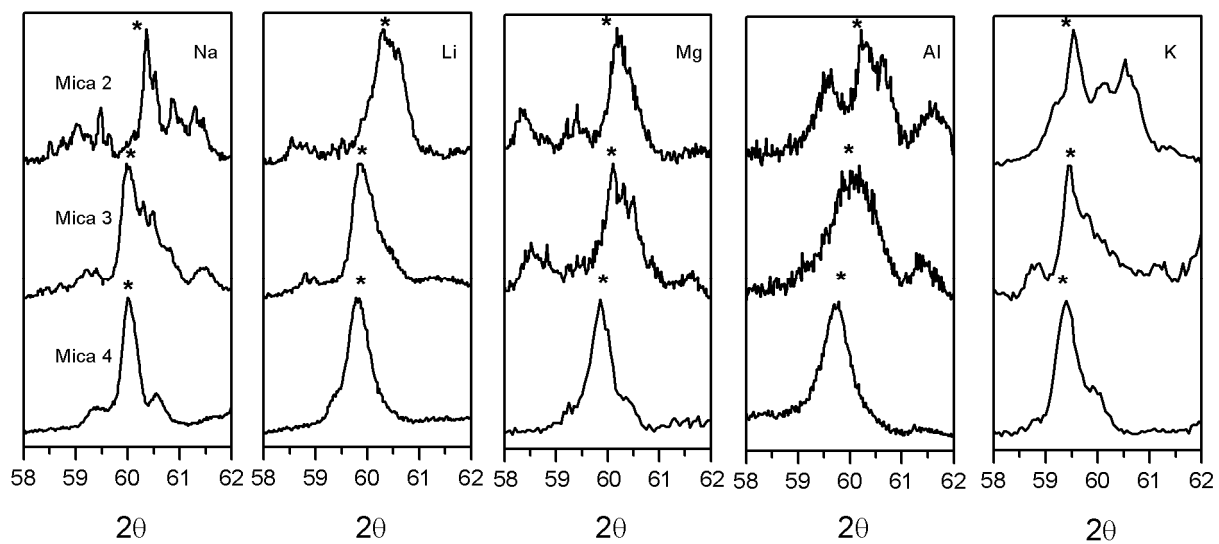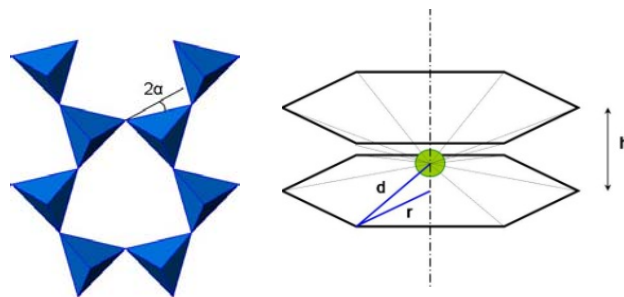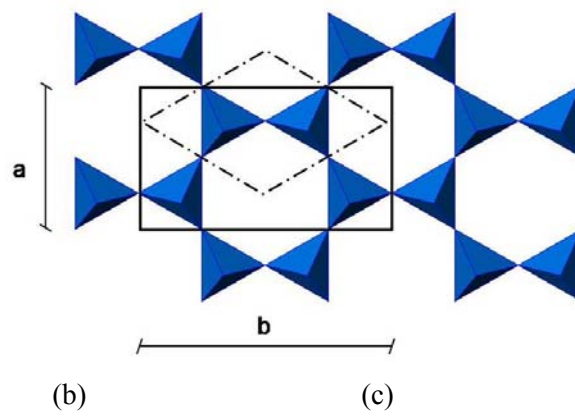**Figure 7.** ^{27}Al MAS-NMR spectra of X-Mica-n.
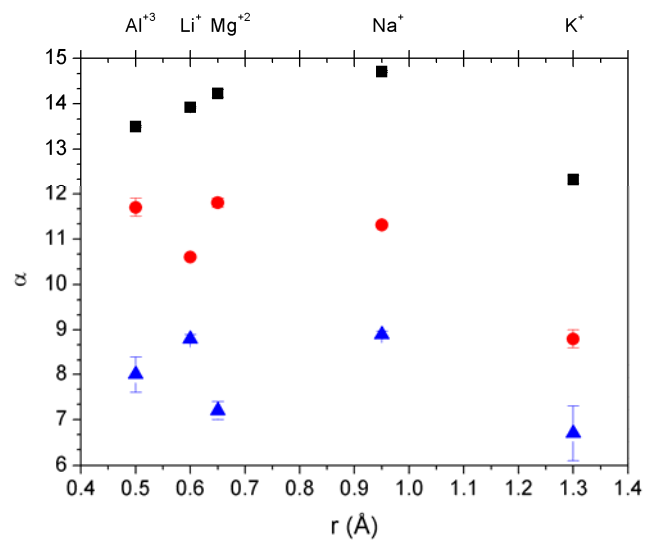
Figure 1

Figure 2

(b)   (c)
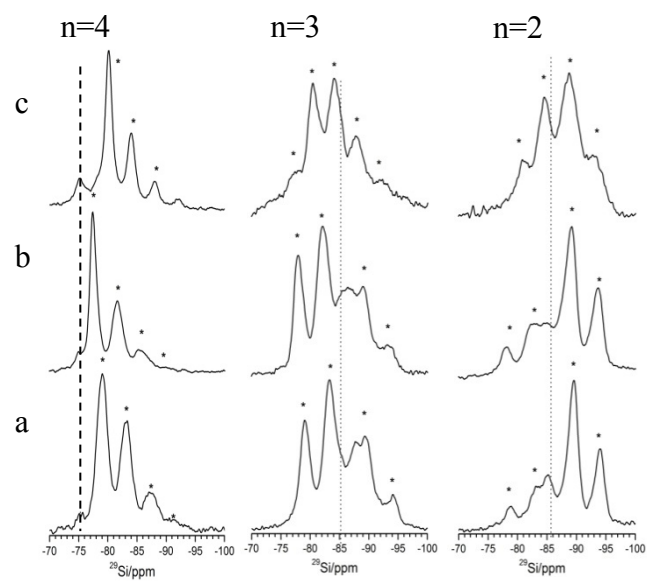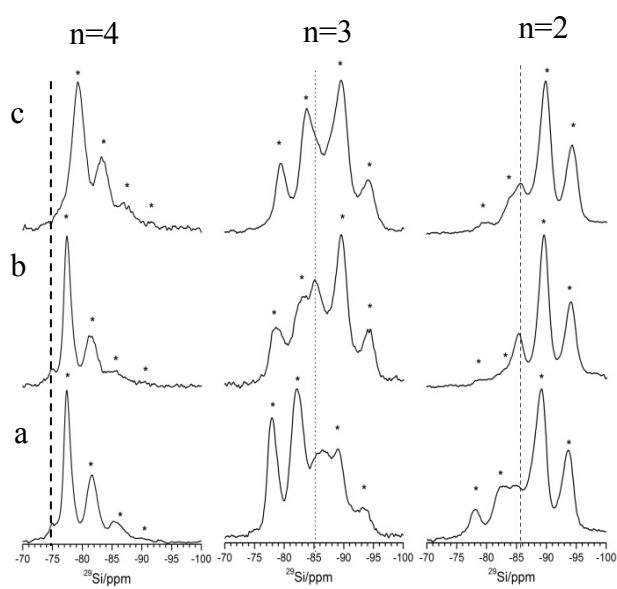
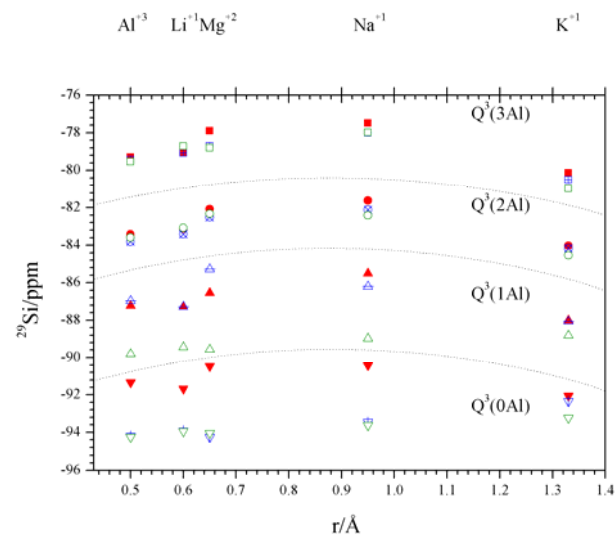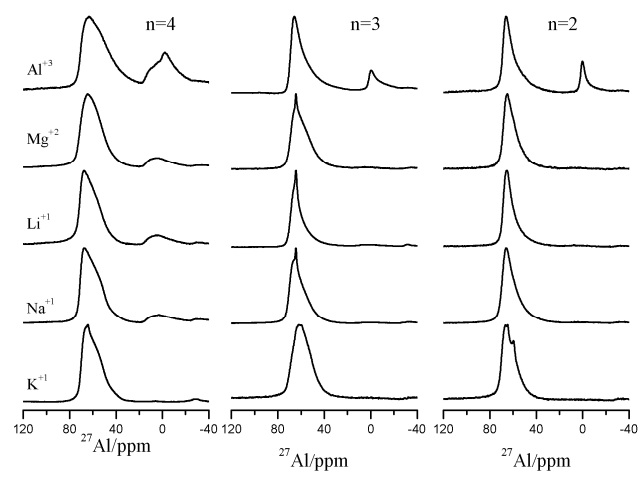*Figure 3*

Figure 4

Figure 5

Figure 6

Figure 7

EXPERIMENTAL

Sample Characterization.

X-ray diffraction (XRD) patterns were measured at the CITIUS X-ray laboratory (University of Seville, Spain) using a Bruker D8 Advance instrument equipped with a Cu K$_\alpha$ radiation source, operating at 40 kV and 40 mA, and with a Ni filter. The powder XRD patterns were registered in the 2θ-range 3–70° with a step size of 0.05° and a time step of 0.03 s.

Figure 1S: X-ray diffractograms obtained for the starting samples- Na-mica-n

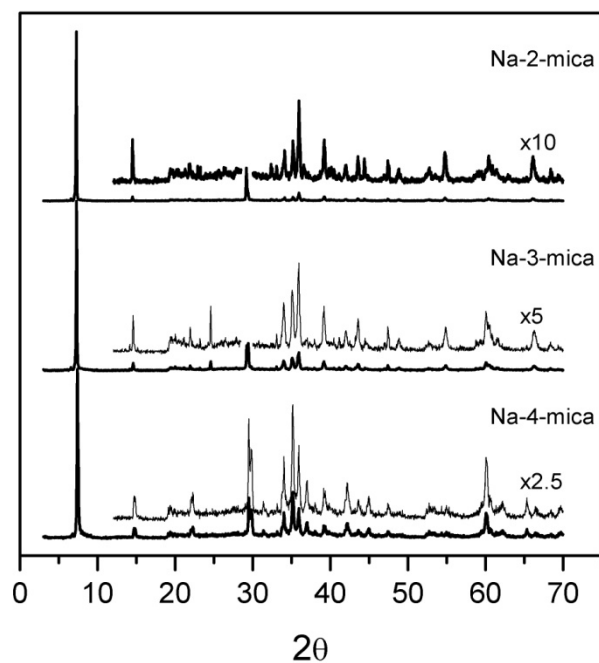**Figure 2S:** X-ray diffractograms obtained for the starting samples homoionized with Li^+, K^+, Mg^{+2} and Al^{+3} cations.